Computer Physics Communications 286 (2023) 108684

Contents lists available at ScienceDirect

Computer Physics Communications

journal homepage: www.elsevier.com/locate/cpc

Compatibility of DFT+U with non-collinear magnetism and spin-orbit coupling within a framework of numerical atomic orbitals ☆

Fernando Gómez-Ortiz [a], Nayara Carral-Sainz [a], James Sifuna [b,c], Virginia Monteseguro [a], Ramón Cuadrado [d], Pablo García-Fernández [a], Javier Junquera [a,*]

[a] Departamento de Ciencias de la Tierra y Física de la Materia Condensada, Universidad de Cantabria, Cantabria Campus Internacional, Avenida de los Castros s/n, 39005 Santander, Spain
[b] Department of Natural Science, The Catholic University of Eastern Africa, 62157-00200, Nairobi, Kenya
[c] School of Physics and Earth Sciences, The Technical University of Kenya, 52428-00200, Nairobi, Kenya
[d] School of Chemistry, University of Southampton, Highfield, Southampton, SO17 1BJ, United Kingdom

ARTICLE INFO

Article history:
Received 1 August 2022
Received in revised form 23 December 2022
Accepted 29 January 2023
Available online 1 February 2023

Keywords:
DFT+U
Spin-orbit
Non-collinear magnetism
Numerical atomic orbitals
SIESTA

ABSTRACT

We report the extension of the density-functional theory plus Hubbard U (DFT+U) method to the case of non-collinear magnetism and spin-orbit coupling in a framework of numerical atomic orbitals. Both the Hubbard repulsion term U, and the exchange J parameters are explicitly included and treated separately. The occupation numbers of the localized orbitals belonging to the correlated shell are computed from the projections of the Kohn-Sham eigenfunctions onto a set of non-overlapping, orthogonal, localized projectors. We provide the detailed expressions for the total energy, forces and stresses including the Pulay corrections. Our implementation on the version 5.0 of the SIESTA package has been validated with simulations carried out in isolated atoms and bulk solids including atoms with a strong spin-orbit coupling.

1. Introduction

Since the advent of the density functional theory (DFT) in the mid-sixties [1,2], this method has become the most widely used framework for first-principles material simulations. Although the exact expression of the total energy functional is unknown, some of its properties are well characterized. One of them is the piece-wise linear dependency of the total energy with respect to the number of electrons (N): the energy profile should consist of a series of straight segments joining the energies corresponding to integer occupations [3]. This fact immediately translates to the appearance of discontinuities in the derivative of the energy as a function of the number of electrons at integral values of N. The discontinuities also appear in the one-electron potential, defined as the functional derivative of the total energy with respect to the electron density, and are responsible for large contributions in the opening of band gaps [4].

Some of the actual and most extended approximations to the DFT, such as the local density approximation (LDA; based on the homogeneous electron gas limit), does not present such discontinuities: the approximated energy functional is continuous with all the derivatives continuous as a function of N. Besides, these approximate functionals fail to cancel out the electronic self-interaction contained in the classical Hartree term (portions of the charge density associated with the same electron repel each other), producing over-delocalization of the valence electrons and the over-stabilization of metallic ground states. As a result, LDA fails while describing band gaps of Mott insulators or other systems with localized electrons.

A correction was proposed by Anisimov and coworkers [5] by adding an orbital-dependent correction to LDA potentials (the so-called LDA+U method), that allowed the orbital polarization and the Mott-Hubbard gap opening in the single-particle spectrum. The main idea behind the method is to separate the electrons in two subsystems: the "strongly correlated" electronic states (typically, localized d or f orbitals) using the Hubbard model, whereas the rest of the delocalized valence electrons are described at the level of "standard"

☆ The review of this paper was arranged by Prof. Blum Volker.

* Corresponding author.
E-mail address: javier.junquera@unican.es (J. Junquera).

https://doi.org/10.1016/j.cpc.2023.108684

approximate orbital-independent one-electron potential coming from DFT functionals. Exchange and non-sphericity of the interactions were later included by Anisimov *et al.* in Ref. [6]. Finally, a unitary-transformation-invariant formulation of LDA+U was introduced in Ref. [7], borrowing expressions for the energy from Hartree-Fock theory. Within this methodology, the total energy of the system is written as

$$E^{\mathrm{DFT+U}}\left[\rho^{\sigma}(\mathbf{r}), n^{I,\sigma}_{mm'}\right] = E^{\mathrm{DFT}}\left[\rho^{\sigma}(\mathbf{r})\right] + E^{\mathrm{Hub}}\left[\{n^{I,\sigma}_{mm'}\}\right] - E^{\mathrm{dc}}\left[\{n^{I,\sigma}\}\right]. \tag{1}$$

In Eq. (1), E^{DFT} is the total energy coming from the approximated DFT functional, that can be computed from the charge density for the spin-σ. E^{Hub} is the term that contains the Hubbard Hamiltonian to model correlated states. Finally, we have to subtract from the approximate DFT functional the part of the interaction energy that will be directly taken into account by E^{Hub}. This is done with the double-counting term E^{dc}. $n^{I,\sigma}_{mm'}$ are occupation numbers of localized orbitals states.

A few years later, Dudarev *et al.* [8] proposed a simplified rotationally invariant expression of the Hubbard plus the double counting terms, where the exchange parameter J was set to zero, and the Coulomb interaction is introduced through an effective $U_{\mathrm{eff}} = U - J$. This simplified version becomes very popular because it produces similar results as the fully rotational invariant formulation [7]. However, some works have pointed the inadequacy of neglecting the explicit dependence on the exchange interaction J to deal with non-collinear magnetism [9] or other systems subject to spin-orbit coupling.

It is not the goal of this paper to review all the approaches that have appeared to overcome the problem of making DFT+U compatible with spin-orbit coupling, including different choices of the double-counting correction terms in Eq, (1). We address the attention of the interested reader to more comprehensive reviews, such as the one in Ref. [10]. Our goal is to explain how the formalism presented in Ref. [9] has been adapted to the framework of a numerical atomic orbital method, as implemented in SIESTA code [11,12]. Similar approaches have recently appeared in the literature, related with other codes such as OPENMX [13], or ABACUS [14].

The rest of the paper is organized as follows. In Sec. 2 we explain the methodology behind the approach for the case of collinear magnetism, to set up the notation and to clarify some of the concepts in an easier environment. The Hubbard and double-counting contribution (within the fully localized limit) to the self-consistent potential are described in Sec. 2.1.1 and Sec. 2.1.2, respectively. A practical equation to compute the total energy coming from the Hubbard and double-counting contribution is presented in Sec. 2.1.3. The corresponding generalizations to the case of non-collinear magnetism, following the recipe given in Ref. [9], is the topic of Sec. 2.2. In Sec. 2.3 we summarize how the integrals related with the on-site electron-electron interactions are computed. The contribution to the forces is given in Sec, 2.4. Finally, we validate the implementation (available in the version 5.0 of the SIESTA code) with two practical examples (an isolated atom and a solid) in Sec. 3.

2. Methods

2.1. Collinear magnetism

2.1.1. The Hubbard contribution to the self-consistent potential

The starting point is the Hubbard Hamiltonian to model correlated states proposed by Liechtenstein and coworkers [7]

$$\begin{aligned} E^{\mathrm{Hub}}\left[\{n^{I,\sigma}_{mm'}\}\right] = \frac{1}{2}\sum_{I}\sum_{\sigma}\sum_{\{m\}}\{&\langle m, m''|V_{\mathrm{ee}}|m', m'''\rangle n^{I,\sigma}_{mm'} n^{I,-\sigma}_{m''m'''} \\ &+ \left(\langle m, m''|V_{\mathrm{ee}}|m', m'''\rangle\right. \\ &\left. - \langle m, m''|V_{\mathrm{ee}}|m''', m'\rangle\right) n^{I,\sigma}_{mm'} n^{I,\sigma}_{m''m'''}\}, \end{aligned} \tag{2}$$

where, following the notation of Ref. [10], I runs over atoms, located at $\mathbf{R}_I$, containing correlated shell of electrons, the state index m runs over the eigenstates of L_z for a given angular quantum number l, and σ refers to the spin of the electron. The V_{ee} integrals represent electron–electron interactions that are expressed as the integrals of the Coulomb kernel on the wave functions of the correlated shell. We shall devote Sec. 2.3 to explain in detail how they are estimated. It is important to note how self-interaction is absent in the Hubbard energy given in Eq. (2).

Within SIESTA, the occupations $n^{I,\sigma}_{mm'}$ are computed from the projections of Kohn-Sham eigenfunctions onto a set of non-overlapping (i.e. orthogonal) localized projectors $|\phi^I_m\rangle$, as

$$\begin{aligned} n^{I,\sigma}_{mm'} &= \langle \phi^I_m|\hat{\rho}^{\sigma}|\phi^I_{m'}\rangle \\ &= \sum_{\mathbf{k}}\sum_{i}\langle\phi^I_m|\psi^{\sigma}_{\mathbf{k}i}\rangle f^{\sigma}_{\mathbf{k}i}\langle\psi^{\sigma}_{\mathbf{k}i}|\phi^I_{m'}\rangle, \end{aligned} \tag{3}$$

where $f^{\sigma}_{\mathbf{k}i}$ represents the occupation of the Kohn-Sham states, labeled by $\mathbf{k}$-point, band i, and spin σ indices, and we have defined the one-particle density operator, $\hat{\rho}^{\sigma}$, as $\hat{\rho}^{\sigma} = \sum_{\mathbf{k}}\sum_i |\psi^{\sigma}_{\mathbf{k}i}\rangle f^{\sigma}_{\mathbf{k}i}\langle\psi^{\sigma}_{\mathbf{k}i}|$. Practically, these projectors can be computed in the same way as the numerical atomic orbitals of the basis set, but with shorter ranges. This differs from the Mulliken charge projector algorithm followed in Ref. [13], and Ref. [14].

In SIESTA [11], the Bloch eigenstates are expanded as a linear combination of strictly localized numerical atomic orbitals, ϕ_μ, as

$$\psi^{\sigma}_{\mathbf{k}i}(\mathbf{r}) = \sum_{\mu} e^{i\mathbf{k}\cdot\mathbf{R}_\mu} c^{\sigma}_{\mu i}(\mathbf{k})\phi_\mu(\mathbf{r}), \tag{4}$$

where $\mu \equiv \{Ilm\zeta\}$, with ζ being the index that label the functions with the same angular dependence (determined by l, and m) but different radial dependency, $c^{\sigma}_{\mu i}(\mathbf{k}) = \langle\phi^{\mu}|\psi^{\sigma}_{\mathbf{k}i}\rangle$, and ϕ^{μ} is the dual orbital of ϕ_μ, $\langle\phi^{\mu}|\phi_\nu\rangle = \delta_{\mu\nu}$. Thus, introducing twice the projector operator into the space spanned by the numerical atomic orbitals basis set, the populations of Eq. (3) can be computed as

$$
\begin{aligned}
n^{I,\sigma}_{mm'} &= \langle \phi^I_m | \left(\sum_\mu |\phi_\mu\rangle\langle\phi^\mu| \right) |\hat{\rho}^\sigma| \left(\sum_\nu |\phi^\nu\rangle\langle\phi_\nu| \right) |\phi^I_{m'}\rangle \\
&= \sum_{\mu\nu} \langle \phi^I_m|\phi_\mu\rangle\langle\phi^\mu|\hat{\rho}^\sigma|\phi^\nu\rangle\langle\phi_\nu|\phi^I_{m'}\rangle \\
&= \sum_{\mu\nu} \langle \phi^I_m|\phi_\mu\rangle \rho^\sigma_{\mu\nu} \langle\phi_\nu|\phi^I_{m'}\rangle \\
&= \sum_{\mu\nu} S^I_{m\mu}\rho^\sigma_{\mu\nu} S^{\ I}_{\nu m'},
\end{aligned} \tag{5}
$$

where the density matrix elements are written in terms of the duals of the numerical atomic orbitals [15] ($\rho^\sigma_{\mu\nu} = \langle\phi^\mu|\hat{\rho}^\sigma|\phi^\nu\rangle$) and we have introduced the notation $S^I_{m\mu} = \langle\phi^I_m|\phi_\mu\rangle$ to denote the overlap between the projectors used to compute the occupations and the atomic orbitals of the basis.

Replacing Eq. (5) into Eq. (2) we arrive to the following expression for the Hubbard energy

$$
E^{\text{Hub}} = \frac{1}{2}\sum_{\mu\nu}\sum_\sigma V^{\text{Hub},\sigma}_{\nu\mu}\rho^\sigma_{\mu\nu} = \frac{1}{2}\sum_\sigma \text{Tr}\left(\hat{V}^{\text{Hub},\sigma}\hat{\rho}^\sigma\right), \tag{6}
$$

where

$$
\begin{aligned}
V^{\text{Hub},\sigma}_{\nu\mu} = \sum_I \sum_{\{m\}} \Big[&\langle m, m''|V_{\text{ee}}|m', m'''\rangle \left(n^{I,-\sigma}_{m''m'''} + n^{I,\sigma}_{m''m'''} \right) \\
&- \langle m, m''|V_{\text{ee}}|m''', m'\rangle n^{I,\sigma}_{m''m'''} \Big] \left(S^I_{m\mu} S^{\ I}_{\nu m'} \right).
\end{aligned} \tag{7}
$$

This potential must be added to the usual DFT effective single particle potential in the self-consistency procedure. It is important to notice how there might be non-zero potential matrix elements, $V^{\text{Hub},\sigma}_{\nu\mu}$, even between pairs of orbitals ν and μ that do not belong to the correlated subspace. If the basis set would be orthonormal with the projectors, then $\langle\phi^I_m|\phi_\mu\rangle = \delta^I_{m\mu}$, and $\langle\phi_\nu|\phi^I_{m'}\rangle = \delta^{\ I}_{\nu m'}$, and Eq. (7) would transform into the expression given in Eq. (3) of Ref. [9].

2.1.2. The double-counting contribution to the self-consistent potential

Besides the Hubbard contribution, we have to consider the double-counting energy that, following Eq. (13) of Ref. [16], in the fully localized limit takes the form

$$
E^{\text{dc}} = \frac{1}{4}\sum_I \left[2U^I n^I (n^I - 1) - 2J^I n^I \left(\frac{n^I}{2} - 1 \right) - J^I \mathbf{m}^I \cdot \mathbf{m}^I \right], \tag{8}
$$

where

$$
n^I = \sum_\sigma \sum_m n^{I\sigma}_{mm}. \tag{9}
$$

Assuming collinear spin, then $\mathbf{m}^I = \left(0, 0, m^I_z\right) = \left(0, 0, n^{I,\uparrow} - n^{I,\downarrow}\right)$, so Eq. (8) reduces to

$$
E^{\text{dc}} = \sum_I \left[\frac{U^I}{2} n^I (n^I - 1) - \frac{J^I}{2} \left[n^{I,\uparrow}\left(n^{I,\uparrow} - 1\right) + n^{I,\downarrow}\left(n^{I,\downarrow} - 1\right) \right] \right], \tag{10}
$$

that corresponds with the double counting term of Eq. (4) in Ref. [7]. Replacing Eq. (9) into Eq. (10), and taking the functional derivatives with respect to the density matrix, we arrive to the contributions of the double-counting terms to the self-consistent potential

$$
\begin{aligned}
V^{\text{dc},\sigma}_{\nu\mu} =& \frac{\delta E^{\text{dc}}}{\delta \rho^\sigma_{\mu\nu}} \\
=& \sum_I \sum_m U^I \left(S^I_{m\mu} S^{\ I}_{\nu m} \right) \left(n^I - \frac{1}{2} \right) \\
&- \sum_I J^I \left[\left(\sum_m \left(S^I_{m\mu} S^{\ I}_{\nu m} \right) \right) \left(\sum_{m'} \sum_{\mu'\nu'} \rho^\sigma_{\mu'\nu'} S^I_{m'\mu'} S^{\ I}_{\nu' m'} - \frac{1}{2} \right) \right].
\end{aligned} \tag{11}
$$

2.1.3. Contribution to the energy

The contribution to the total energy can be computed from a direct evaluation of Eq. (2) and Eq. (8) for the Hubbard and double-counting contributions, respectively. Alternatively, it can be written as the half trace of the product of the potential times the density matrix plus some correction terms, as

$$E^{\mathrm{Hub}} - E^{\mathrm{dc}} = \frac{1}{2}\sum_{\sigma} \mathrm{Tr}\left[\left(V^{\mathrm{Hub},\sigma} + V^{\mathrm{dc},\sigma}\right)\rho^{\sigma}\right] - \sum_{I}\frac{1}{4}\left(U^{I} - J^{I}\right)n^{I}. \tag{12}$$

2.2. Non collinear magnetism

2.2.1. The Hubbard and double-counting contributions to the self-consistent potential

The previous formalism for collinear spins can be extended to the case of noncollinear magnetism. In this case, we have to take into account that the density matrix between two atomic orbitals μ and ν is a complex (2×2) matrix

$$\rho_{\mu\nu} = \begin{pmatrix} \rho_{\mu\nu}^{\uparrow\uparrow} & \rho_{\mu\nu}^{\uparrow\downarrow} \\ \rho_{\mu\nu}^{\downarrow\uparrow} & \rho_{\mu\nu}^{\downarrow\downarrow} \end{pmatrix}. \tag{13}$$

This immediately translates into the fact that the occupations introduced in Eq. (5) are also complex (2×2) matrices,

$$n^{I}_{mm'} = \begin{pmatrix} n^{I,\uparrow\uparrow}_{mm'} & n^{I,\uparrow\downarrow}_{mm'} \\ n^{I,\downarrow\uparrow}_{mm'} & n^{I,\downarrow\downarrow}_{mm'} \end{pmatrix}. \tag{14}$$

From this, the total number of correlated electrons, n^I, and the magnetic moment, $\mathbf{m}^I$, of every individual atom I can be computed as

$$n^{I} = \sum_{m}\mathrm{Tr}\left(\mathbb{1}n^{I}_{mm}\right) = \sum_{m}\left(n^{I\uparrow\uparrow}_{mm} + n^{I\downarrow\downarrow}_{mm}\right), \tag{15a}$$

$$m^{I}_{x} = \sum_{m}\mathrm{Tr}\left(\sigma_x n^{I}_{mm}\right) = \sum_{m}\left(n^{I\uparrow\downarrow}_{mm} + n^{I\downarrow\uparrow}_{mm}\right), \tag{15b}$$

$$m^{I}_{y} = \sum_{m}\mathrm{Tr}\left(\sigma_y n^{I}_{mm}\right) = \sum_{m} i\left(n^{I\uparrow\downarrow}_{mm} - n^{I\downarrow\uparrow}_{mm}\right), \tag{15c}$$

$$m^{I}_{z} = \sum_{m}\mathrm{Tr}\left(\sigma_z n^{I}_{mm}\right) = \sum_{m}\left(n^{I\uparrow\uparrow}_{mm} - n^{I\downarrow\downarrow}_{mm}\right), \tag{15d}$$

where σ_x, σ_y, and σ_z representing the (2×2) Pauli matrices. The generalization of the DFT+U potential, also expressed in the two-component spin space as,

$$V_{\nu\mu} = \begin{pmatrix} V_{\nu\mu}^{\uparrow\uparrow} & V_{\nu\mu}^{\uparrow\downarrow} \\ V_{\nu\mu}^{\downarrow\uparrow} & V_{\nu\mu}^{\downarrow\downarrow} \end{pmatrix}, \tag{16}$$

was done by Bousquet and Spaldin [9]. Every potential matrix element is the sum of the corresponding Hubbard and double-counting contribution. Each element of the (2×2) matrix can be computed as a functional derivative of the energy with respect to the corresponding density matrix term

$$V_{\nu\mu}^{\alpha\beta} = \frac{\delta E}{\delta \rho_{\mu\nu}^{\beta\alpha}}. \tag{17}$$

For the diagonal components, they are the same as the ones obtained in Eq. (7) and Eq. (11) of Sec. 2.1, respectively, and can be generalized as

$$V_{\nu\mu}^{\mathrm{Hub},\uparrow\uparrow(\downarrow\downarrow)} = \sum_{I}\sum_{\{m\}}\Big[\langle m, m''|V_{\mathrm{ee}}|m', m'''\rangle\left(n^{I,\downarrow\downarrow}_{m''m'''} + n^{I,\uparrow\uparrow}_{m''m'''}\right) - \langle m, m''|V_{\mathrm{ee}}|m''', m'\rangle n^{I,\uparrow\uparrow(\downarrow\downarrow)}_{m''m'''}\Big]\left(S^{I}_{m\mu}S^{\ I}_{\nu m'}\right), \tag{18a}$$

$$V_{\nu\mu}^{\mathrm{dc},\uparrow\uparrow(\downarrow\downarrow)} = \sum_{I}\sum_{m}U^{I}\left(S^{I}_{m\mu}S^{\ I}_{\nu m}\right)\left(n^{I} - \frac{1}{2}\right) - \sum_{I}J^{I}\left[\left(\sum_{m}\left(S^{I}_{m\mu}S^{\ I}_{\nu m}\right)\right)\left(\sum_{m'}\sum_{\mu'\nu'}\rho^{\uparrow\uparrow(\downarrow\downarrow)}_{\mu'\nu'}S^{I}_{m'\mu'}S^{\ I}_{\nu' m'} - \frac{1}{2}\right)\right], \tag{18b}$$

For the off-diagonal terms, we follow the expressions given by Bousquet and Spaldin in Ref. [9]

$$V_{\nu\mu}^{\mathrm{Hub},\uparrow\downarrow(\downarrow\uparrow)} = -\sum_{I}\sum_{\{m\}}\Big[\langle m, m''|V_{\mathrm{ee}}|m''', m'\rangle n^{I,\uparrow\downarrow(\downarrow\uparrow)}_{m''m'''}\Big]S^{I}_{m\mu}S^{\ I}_{\nu m'}, \tag{19a}$$

$$V_{\nu\mu}^{\mathrm{dc},\uparrow\downarrow(\downarrow\uparrow)} = -\sum_{I}J^{I}\left[\left(\sum_{m}\left(S^{I}_{m\mu}S^{\ I}_{\nu m}\right)\right)\left(\sum_{m'}\sum_{\mu'\nu'}\rho^{\uparrow\downarrow(\downarrow\uparrow)}_{\mu'\nu'}S^{I}_{m'\mu'}S^{\ I}_{\nu' m'}\right)\right], \tag{19b}$$

Both the Hubbard and the double counting matrix elements must be computed self-consistently. It is important to note here how both the potential [Eq. (16)] and the density matrix [Eq. (13)] are globally Hermitian ($\rho_{\mu\nu}^{\alpha\beta} = \rho_{\nu\mu}^{\beta\alpha *}$).

2.2.2. Contribution to the energy

The contribution to the energy can be computed following the Eq. (12), but now the trace has to be extended to the multiplication of the (2×2) matrices as

$$E^{\text{Hub}} - E^{\text{dc}} = \frac{1}{2} \sum_{\mu\nu} \left(\rho_{\mu\nu}^{\uparrow\uparrow} V_{\nu\mu}^{\uparrow\uparrow} + \rho_{\mu\nu}^{\uparrow\downarrow} V_{\nu\mu}^{\downarrow\uparrow} + \rho_{\mu\nu}^{\downarrow\uparrow} V_{\nu\mu}^{\uparrow\downarrow} + \rho_{\mu\nu}^{\downarrow\downarrow} V_{\nu\mu}^{\downarrow\downarrow} \right) - \sum_{I} \frac{1}{4} \left(U^I - J^I \right) n^I. \tag{20}$$

In Eq. (20) we have considered that $V_{\nu\mu}$ is the sum of the Hubbard and the double-counting contributions.

2.3. Integrals of the electron-electron interaction

In the previous Sections, the integrals related with the electron-electron interaction,

$$\langle m, m'' | V_{\text{ee}} | m', m''' \rangle = \int d^3r \int d^3r' \psi_{lm}^*(\mathbf{r}) \psi_{lm''}^*(\mathbf{r}') \frac{e^2}{|\mathbf{r} - \mathbf{r}'|} \psi_{lm'}(\mathbf{r}) \psi_{lm'''}(\mathbf{r}'), \tag{21}$$

remain to be determined. Here we follow the recipe given in Ref. [7]. Assuming that the functions of the kind ψ_{lm} involved in Eq. (21) are atomic-like d or f states, then they can be written as the product of a radial part times a *real* spherical harmonic, that can be trivially expressed as a linear combination of *complex* spherical harmonics. The Coulomb kernel can also be expanded in a basis of *complex* spherical harmonics as [17],

$$\frac{e^2}{|\mathbf{r} - \mathbf{r}'|} = 4\pi e^2 \sum_{l=0}^{\infty} \sum_{m=-l}^{l} \frac{1}{2l+1} \frac{r_<^l}{r_>^{l+1}} Y_{lm}^*(\theta', \phi') Y_{lm}(\theta, \phi), \tag{22}$$

where $r_<$ (respectively $r_>$) is the smaller (respectively larger) of $|\mathbf{r}|$ and $|\mathbf{r}'|$. Then, the electron-electron interaction integrals can be factorized in the product of a radial and an angular contribution

$$\langle m, m'' | V_{\text{ee}} | m', m''' \rangle = \sum_k a_k(m, m', m'', m''') F^k, \tag{23}$$

where k is an even integer in the range $0 \leq k \leq 2l$, with l being the angular momentum number of the localized manifold with $-l \leq m \leq l$.

2.3.1. Angular contribution

The a_k terms in Eq. (23) represent the angular factors and corresponds to products of three complex spherical harmonics (Gaunt coefficients)

$$a_k(m, m', m'', m''') = \frac{4\pi}{2k+1} \sum_{q=-k}^{k} \langle lm | Y_{kq} | lm' \rangle \langle lm'' | Y_{kq}^* | lm''' \rangle, \tag{24}$$

that can be simplified as a simple expression involving only a normalization constant and two Wigner $3j$ symbols,

$$\begin{aligned} \langle lm | Y_{kq} | lm' \rangle &= \int_0^{2\pi} \int_0^{\pi} Y_{l,m}^*(\theta, \phi) Y_{k,q}(\theta, \phi) Y_{l,m'}(\theta, \phi) \sin\theta d\theta d\phi \\ &= \int_0^{2\pi} \int_0^{\pi} (-1)^m Y_{l,-m}(\theta, \phi) Y_{k,q}(\theta, \phi) Y_{l,m'}(\theta, \phi) \sin\theta d\theta d\phi \\ &= (-1)^m \sqrt{\frac{(2l+1) \times (2k+1) \times (2l+1)}{4\pi}} \begin{pmatrix} l & k & l \\ 0 & 0 & 0 \end{pmatrix} \begin{pmatrix} l & k & l \\ -m & q & m' \end{pmatrix}. \end{aligned} \tag{25}$$

A similar expression is obtained for the second product of the three spherical harmonics in Eq. (24). The Gaunt integrals are different from zero if and only if $q + m' = m \Rightarrow q = m - m'$, and $-q + m''' = m'' \Rightarrow q = m''' - m''$. The 3-$j$ symbols are given in terms of the Clebsch–Gordan coefficients by

$$\begin{pmatrix} j_1 & j_2 & j_3 \\ m_1 & m_2 & m_3 \end{pmatrix} \equiv \frac{(-1)^{j_1 - j_2 - m_3}}{\sqrt{2j_3 + 1}} \langle j_1 m_1 j_2 m_2 | j_3 (-m_3) \rangle, \tag{26}$$

where the Clebsch–Gordan coefficients can be taken from the Racah formula [18].

Finally, Eq. (24) transforms into [7]

$$a_k(m,m',m'',m''') = \sum_{q=-k}^{k} (2l+1)^2(-1)^{m+q+m''} \times \begin{pmatrix} l & k & l \\ 0 & 0 & 0 \end{pmatrix}^2 \begin{pmatrix} l & k & l \\ -m & q & m' \end{pmatrix} \times \begin{pmatrix} l & k & l \\ -m'' & -q & m''' \end{pmatrix}. \tag{27}$$

2.3.2. Radial contribution

The quantities F^k in Eq. (23) are the Slater integrals involving the radial part of the atomic wave functions R_{nl} (n indicating the atomic shell they belong to). They have the following expression [10]

$$F^k = e^2 \int d^3r \int d^3r' r^2 r'^2 R_{nl}^2(r) \frac{r_<^k}{r_>^{k+1}} R_{nl}^2(r'). \tag{28}$$

For d electrons, only F^0, F^2, and F^4 are needed to compute the V_{ee} matrix elements (for higher k values the corresponding a_k vanish), while the f electrons also require F^6.

In practice, the Slater integrals given in Eq. (28) are not computed. They can be estimated from the Coulomb U and Stoner J parameters through [7]

$$U = F^0, \tag{29a}$$

$$J = \frac{F^2 + F^4}{14}, \tag{29b}$$

while the ratio $F^4/F^2 = 0.625$ is taken as a constant, a good approximation for d-electron systems [7] (the ratio between F^4 and F^2 for all the $3d$ ions is between 0.62 and 0.63 [19]). Therefore, given U and J as parameters,

$$F^0 = U, \tag{30a}$$

$$F^2 = \frac{14 \times J}{(1 + 0.625)}, \tag{30b}$$

$$F^4 = 0.625 \times F^2. \tag{30c}$$

Similarly, for f-orbitals the ratio of F^4 and F^6 with respect to F^2 can be fixed, respectively to, $F^4/F^2 \approx 0.67$ and $F^6/F^2 \approx 0.49$ [20]. The U and J parameters are given in these cases as,

$$U = F^0, \tag{31a}$$

$$J = \frac{286F^2 + 195F^4 + 250F^6}{6435}, \tag{31b}$$

and writing U and J in terms of the Slater integrals,

$$F^0 = U, \tag{32a}$$

$$F^2 = \frac{6435}{286 + 195 \times 0.67 + 250 \times 0.49} J, \tag{32b}$$

$$F^4 = 0.67 \times F^2, \tag{32c}$$

$$F^6 = 0.49 \times F^2. \tag{32d}$$

Once the electron-electron interaction integrals [Eq. (23)] are computed in a basis of complex spherical harmonics from the expressions given in Eq. (27) (angular contribution) and Eqs. (30a)-(30c) [radial contribution, alternatively for f-orbitals Eqs. (32a)-(32c)], then we can transform back to a basis of real spherical harmonics as the ones used in the expansion of the atomic orbitals.

As a final verification of the implementation, we checked the following average relationships that result from the properties of the Clebsh-Gordan coefficients [6,21]

$$U = \frac{1}{(2l+1)^2} \sum_{m,m'} \langle m, m' | V_{ee} | m, m' \rangle = F^0$$

$$U - J = \frac{1}{2l(2l+1)} \sum_{m,m'} \left(\langle m, m' | V_{ee} | m, m' \rangle - \langle m, m' | V_{ee} | m', m \rangle \right). \tag{33}$$

Table 1
Reference configuration, cutoff radii and matching radius between the full core charge and the partial core charge for the pseudopotentials used in our study. Units are in bohr.

Reference		Ir	O	Mn
		$6s^2, 6p^0, 5d^7, 5f^0$	$2s^2, 2p^4, 3d^0, 4f^0$	$4s^2, 4p^0, 3d^5, 4f^0$
Core radius	s	2.20	1.50	2.00
	p	2.80	1.60	2.00
	d	1.30	1.40	2.00
	f	2.00	1.15	2.00
Relativistic?		yes	yes	yes
Non-linear core corrections (NLCC)?		yes	yes	yes
Matching radius NLCC		1,40	1.20	

2.4. Atomic forces and stresses

Atomic forces and stresses are obtained by direct differentiation of the energy [Eq. (20)] with respect to atomic positions. The Pulay corrections, due to the fact that the basis set functions explicitly depend on the ionic positions, are automatically included. The force terms containing $\partial\rho_{\mu\nu}/\partial\mathbf{R}_K$ are exactly multiplied by the corresponding potential matrix elements. This contribution to the forces takes the shape $\sum_{\mu\nu} V_{\nu\mu}\partial\rho_{\mu\nu}/\partial\mathbf{R}_K$ and, thus, can be computed by the orthogonality forces as explained in Appendix A of Ref. [11]. The remaining contributions to the forces coming from the Hubbard and double counting terms that are explicitly taken into account are summarized below.

$$
\begin{aligned}
F^{\mathrm{Hub}} = &-2\sum_I\sum_{\mu\nu}\sum_{\{m\}}\Big[\langle m,m''|V_{ee}|m',m'''\rangle\left(n^{I,\uparrow\uparrow}_{m''m'''}+n^{I,\downarrow\downarrow}_{m''m'''}\right)\\
&-\langle m,m''|V_{ee}|m''',m'\rangle n^{I,\uparrow\uparrow}_{m''m'''}\Big]\frac{\partial S^I_{m\mu}}{\partial\mathbf{R}_K}S^{\ I}_{\nu m'}\rho^{\uparrow\uparrow}_{\mu\nu}\\
&-2\sum_I\sum_{\mu\nu}\sum_{\{m\}}\Big[\langle m,m''|V_{ee}|m',m'''\rangle\left(n^{I,\uparrow\uparrow}_{m''m'''}+n^{I,\downarrow\downarrow}_{m''m'''}\right)\\
&-\langle m,m''|V_{ee}|m''',m'\rangle n^{I,\downarrow\downarrow}_{m''m'''}\Big]\frac{\partial S^I_{m\mu}}{\partial\mathbf{R}_K}S^{\ I}_{\nu m'}\rho^{\downarrow\downarrow}_{\mu\nu}\\
&+2\sum_I\sum_{\mu\nu}\sum_{\{m\}}\langle m,m''|V_{ee}|m''',m'\rangle\frac{\partial S^I_{m\mu}}{\partial\mathbf{R}_K}S^{\ I}_{\nu m'}\left(n^{I,\uparrow\downarrow}_{m''m'''}\rho^{\downarrow\uparrow}_{\mu\nu}+n^{I,\downarrow\uparrow}_{m''m'''}\rho^{\uparrow\downarrow}_{\mu\nu}\right),\\
F^{\mathrm{dc}} = &\sum_I\sum_{\mu\nu}\sum_m\rho^{\uparrow\uparrow}_{\mu\nu}\frac{\partial S^I_{m\mu}}{\partial\mathbf{R}_K}S^{\ I}_{\nu m}\left[\left(-U^I+J^I\right)+2U^In^I-2J^In^{I,\uparrow\uparrow}\right]\\
&+\sum_I\sum_{\mu\nu}\sum_m\rho^{\downarrow\downarrow}_{\mu\nu}\frac{\partial S^I_{m\mu}}{\partial\mathbf{R}_K}S^{\ I}_{\nu m}\left[\left(-U^I+J^I\right)+2U^In^I-2J^In^{I,\downarrow\downarrow}\right]\\
&-\sum_I\sum_{\mu\nu}\sum_m 2J^I\frac{\partial S^I_{m\mu}}{\partial\mathbf{R}_K}S^{\ I}_{\nu m}\left(\rho^{\uparrow\downarrow}_{\mu\nu}n^{I,\downarrow\uparrow}+\rho^{\downarrow\uparrow}_{\mu\nu}n^{I,\uparrow\downarrow}\right).
\end{aligned}
$$

Following the same spirit, the stress tensor is obtained by a direct differentiation of the energy with respect to the strain tensor. Numerically, they can be computed with a very little extra effort from the calculation of the forces, following the same recipe given in Ref. [11].

3. Results

3.1. Computational details

3.1.1. SIESTA

Exchange and correlation were treated within the generalized gradient approximation (GGA) to the density functional theory (DFT) [1,2]. We used the Perdew-Berke-Ernzerhof (PBE) functional [22] for the Mn atom and with the revised PBEsol functional for bulk IrO_2 [23]. The off-site implementation of the spin-orbit coupling as implemented in Refs. [24,25] has been employed.

Core electrons were replaced by *ab initio* norm conserving pseudopotentials, generated using the Troullier-Martins scheme [26] in the Kleinman-Bylander fully non-local separable representation [27]. The reference configuration and cutoff radii for each angular momentum shell for the pseudopotentials used in this work can be found in Table 1.

The one-electron Kohn-Sham eigenstates were expanded in a basis of strictly localized numerical atomic orbitals [28,29]. For Mn, both single-ζ and double-ζ-polarized basis sets with the default values to define the range of the orbitals were used. For IrO_2, the quality of the basis was fixed to double-ζ-polarized. All the parameters that define the shape and range of the basis functions for Ir and O were obtained by a variational optimization of the enthalpy [30,31] with a pressure of 0.3 GPa.

The electronic density, Hartree, and exchange-correlation potentials, as well as the corresponding matrix elements between orbitals, were calculated in a uniform real-space grid, with an equivalent plane-wave cutoff of 600 Ry in the representation of charge density. In

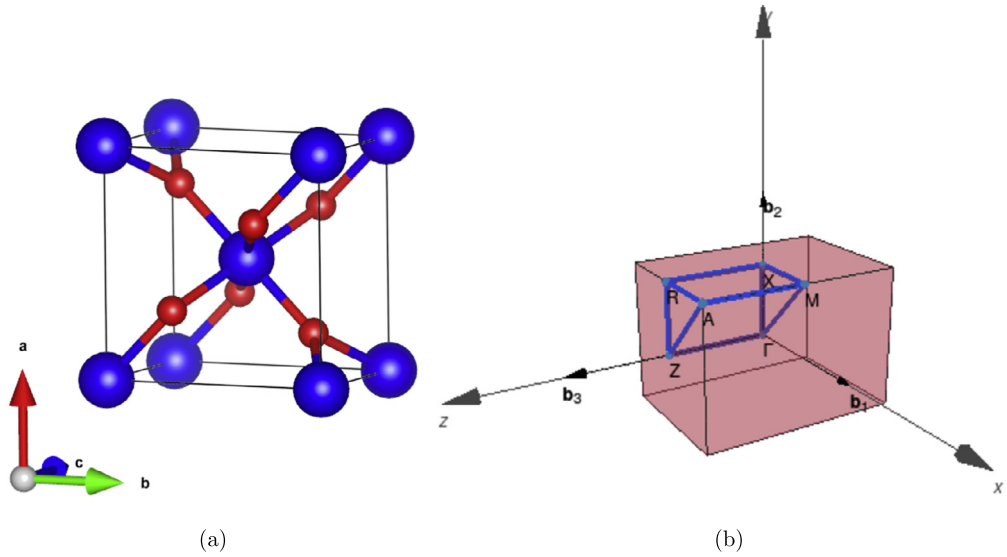

Fig. 1. (a) Crystal structure of simple tetragonal IrO_2. The blue balls represent Ir while the red balls represent O. (b) The primitive Brillouin zone indicating the *k*-path used in this study. The corresponding *k*-path is Γ-X-M-Γ-Z-R-A-M.

the case of bulk IrO_2, for the Brillouin zone integrations we use a Monkhorst-Pack sampling [32] of $8 \times 8 \times 12$ **k**-points. A Fermi-Dirac distribution was chosen for the occupation of the one-particle Kohn-Sham electronic eigenstates, with a very low electronic temperature (1 K).

To simulate the isolated Mn atom, a cubic box of 12 Å of size was defined. For IrO_2, the experimental coordinates taken from Ref. [33,34] in the rutile (tetragonal) structure were chosen as the initial configuration for a conjugate gradient minimization (Fig. 1). Then, the atomic coordinates and the lattice vectors were relaxed until the maximum components of the force on any atom and of the stress tensor were smaller than 10 meV/Å and 1×10^{-4} eV/Å^3, respectively.

For the Mn atom, a Coulomb U = 3.0 eV, and exchange J = 0.3 eV parameters were selected. For bulk IrO_2, in order to correctly describe the correlated Ir 5*d* electrons, the onsite Coulomb interaction U was set to 2 eV and the exchange parameter J to 0 eV. This value, smaller than the typical ones used for 3*d* transition metal oxides, is justified by the spatial extension of the Ir valence 5*d* orbitals. The range of these 5*d* orbitals is comparable to the Ir-O bond distances, so that *d*-*d* overlaps are much larger, yielding to much wider *d* conduction band widths [33].

3.1.2. VASP

Bulk IrO_2 simulations were also carried out using the VASP code [35,36]. Within this framework, the same valence electrons as in Table 1 were retained in the calculation using the projector augmented-wave (PAW) method [37]. Highly converged results were achieved by extending the set of plane waves up to a kinetic energy cutoff of 500 eV. In the relaxed configurations, the forces on the atoms are less than 0.006 eV/Å and the deviation of the stress tensor from a diagonal hydrostatic form is less than 0.1 GPa. The rest of the technicalities were kept the same as for the SIESTA case. The electronic total density of states was calculated by doubling the **k**-points grid used previously for self-consistency. The spin-orbit coupling effect was also included in the density of states and band structure calculation.

3.1.3. QUANTUM ESPRESSO

For further comparison, the simulations on bulk IrO_2 we also carried out with the plane-wave based methodology as implemented in the QUANTUM ESPRESSO package [38,39]. Ultrasoft pseudopotentials [40] taken from the PSLIBRARY [41] were employed, with the same valence configuration as the one shown in Table 1. The kinetic energy cut-off was set to 50 Ry. Full structural optimization including atomic positions were carried out with electronic convergence criteria set to 1.0×10^{-8} eV and the forces optimized to less than 1.0×10^{-6} eV/Å. The rest of the technicalities were kept the same as discussed in Sec. 3.1.1.

3.2. Isolated atoms

As a first trivial test, we have carried out simulations on an isolated Mn atom. The main goal was to check the rotational invariance of the formulation. We confirmed that the total energy was totally independent of the direction of the spin, up to numerical noise smaller than 1 μeV after the self-consistency loops. Different initial spin configurations were tried, differing in the magnitude and direction. While the direction was preserved, the magnitude always saturated to the expected value of 5 μ_B for the d^5 atomic configuration of Mn. Also, imposing a magnetic field through a Zeeman term in the Hamiltonian, we could check how the spin rotated during the self-consistency to align its direction with the external field.

3.3. Bulk IrO_2

We have also relaxed the atomic structure and computed the band structure of bulk IrO_2, one of the most active catalysts for water splitting and the only known catalyst capable of producing O_2 in acidic conditions [33]. The optimized lattice constants and internal parameters of IrO_2 in the rutile structures are shown in Table 2 for different packages, pseudopotentials, basis sets, and functionals.

Table 2
Optimized lattice constants (a, and c), and internal parameter (u) of bulk IrO_2 in the rutile (tetragonal) structure. PW stands for Plane Waves. Units of the lattice constant in Å.

Method	Pseudopotential	Basis set	Functional	a	c	u
SIESTA	Norm-conserving	Local atomic orbitals	PBEsol	4.497	3.164	0.3085
			PBEsol+U	4.503	3.159	0.3081
			PBEsol+U+SOC	4.507	3.159	0.3081
VASP	PAW	PW	PBEsol+U+SOC	4.482	3.150	0.3083
QUANTUM ESPRESSO	Ultrasoft	PW	PBEsol+U+SOC	4.536	3.178	0.3082
CRYSTAL [33]	Core effective potentials	Local atomic orbitals	PBE	4.519	3.196	0.3087
QUANTUM-ESPRESSO [33]	Ultrasoft	PW	PBE	4.538	3.183	0.3083
Experiment [34]				4.505	3.159	0.3077

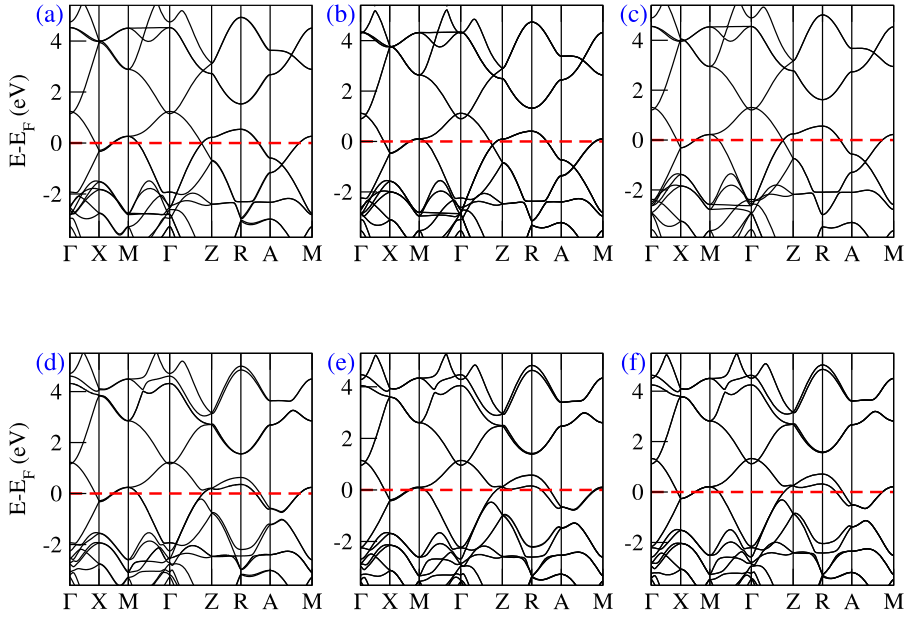

Fig. 2. Band structures of bulk IrO_2 at the theoretical relaxed structures. DFT+U (without spin-orbit) bands are plotted in (a) SIESTA, (b) VASP and (c) QUANTUM ESPRESSO. Once spin-orbit coupling is switched on, the corresponding band structures are replotted in (d) SIESTA, (e) VASP and (f) QUANTUM ESPRESSO. The red dashed horizontal lines correspond to the Fermi energy, E_F, taken to be the origin of energies.

The differences in the lattice constants (internal geometries) differed at most by 1.5% (0.13%) between the different codes, despite the large differences in the methodologies. The relaxed structure obtained within the SIESTA code at 0 K is in very good agreement with the experimental observations at 300 K [34].

The band structure of IrO_2, computed at the relaxed theoretical structure, is shown in Fig. 2. Considering the formal oxidation states, the oxygen atoms would be O^{2-}, while the iridium atoms should be considered as Ir^{4+}. That means that five electrons are expected to occupy the Ir-d levels that are split due to the strong crystal field splitting of the distorted octahedral field into three t_{2g} states and two e_g states. With the t_{2g} band partially occupied (five electrons for a maximum occupancy of six), the Fermi level is expected to cross near the top of the t_{2g} band, making IrO_2 metallic. This metallicity is clearly shown in Fig. 2, in good agreement with previous simulations [42]. The most important effect of the spin-orbit coupling is the lifting of the degeneracy of the bands along the high-symmetry $Z - R - A$ path. Its contribution in other paths is minimal. Therefore, the SOC in bulk IrO_2 is not large enough to yield a splitting of the bands at the Fermi energy, giving rise to a spin-orbit Mott insulating state [42,33]. But, for the purpose of this work, the most important result is the fact that the band structures produced by three different codes such as SIESTA, VASP and QUANTUM ESPRESSO are nearly identical. Very similar results are also obtained with the ABACUS code [14].

4. Conclusions

We have particularized the formalism developed by Bousquet and Spaldin [9] to deal with density-functional theory plus Hubbard U (DFT+U) method for the case of noncollinear magnets to a framework of numerical atomic orbitals. Non-overlapping orthogonal projectors, that can be defined in the same way as the basis atomic orbitals with shorter ranges, are used to map the full Kohn-Sham orbital space into the correlated shell. Expressions for the single-particle potential to be included during the self-consistent cycles, energy and stresses are given. The implementation in the version 5.0 of SIESTA of the former equations are validated in two practical cases. The first is an isolated atom, where the total energy is proven to be independent of the spin direction. The second is the case bulk solid of IrO_2, where the same kind of spin-orbit splitting due to the Ir atom as in former calculations (both with plane waves as in VASP or with numerical atomic orbitals as in ABACUS) are found.

Declaration of competing interest

The authors declare that they have no known competing financial interests or personal relationships that could have appeared to influence the work reported in this paper.

Data availability

Data will be made available on request.

Acknowledgements

We thank B. Amadon for useful discussions and D. Sánchez-Portal for the initial implementation of the LDA+U in SIESTA within the Dudarev approximation. F.G.-O., N.C.-S., P.G.-F., and J.J. acknowledge financial support from Grant No. PGC2018-096955-B-C41 funded by MCIN/AEI/10.13039/501100011033 and by ERDF "A way of making Europe" by the European Union. F.G.-O. acknowledges financial support from Grant No. FPU18/04661 funded by MCIN/AEI/10.13039/501100011033. V. M. acknowledges financial support from Grant No. PID2021-125927NA-C22 funded by MCIN/AEI/10.13039/501100011033 and by ERDF "A way of making Europe" by the European Union, and the Beatriz Galindo Fellowship Grant No. BG20/000777. N.C.-S. acknowledges financial support from "Concepción Arenal" Grant No. BDNS:524538 of the University of Cantabria funded by the Government of Cantabria. The authors acknowledge the computing facilities provided by the Centre for High Performance Computing (CHPC-MATS1424), Cape Town, South Africa.

References

[1] P. Hohenberg, W. Kohn, Phys. Rev. 136 (1964) B864.
[2] W. Kohn, L.J. Sham, Phys. Rev. 140 (1965) A1133.
[3] J.P. Perdew, R.G. Parr, M. Levy, J.L. Balduz, Phys. Rev. Lett. 49 (1982) 1691.
[4] O. Gunnarsson, K. Schönhammer, Phys. Rev. Lett. 56 (1986) 1968.
[5] V.I. Anisimov, J. Zaanen, O.K. Andersen, Phys. Rev. B 44 (1991) 943.
[6] V.I. Anisimov, I.V. Solovyev, M.A. Korotin, M.T. Czyżyk, G.A. Sawatzky, Phys. Rev. B 48 (1993) 16929.
[7] A.I. Liechtenstein, V.I. Anisimov, J. Zaanen, Phys. Rev. B 52 (1995) R5467.
[8] S.L. Dudarev, G.A. Botton, S.Y. Savrasov, C.J. Humphreys, A.P. Sutton, Phys. Rev. B 57 (1998) 1505.
[9] E. Bousquet, N. Spaldin, Phys. Rev. B 82 (2010) 220402.
[10] B. Himmetoglu, A. Floris, S. de Gironcoli, M. Cococcioni, Int. J. Quant. Chem. 114 (2014) 14.
[11] J.M. Soler, E. Artacho, J.D. Gale, A. García, J. Junquera, P. Ordejón, D. Sánchez-Portal, J. Phys. Condens. Matter 14 (2002) 2745.
[12] A. García, N. Papior, A. Akhtar, E. Artacho, V. Blum, E. Bosoni, P. Brandimarte, M. Brandbyge, J.I. Cerdá, F. Corsetti, R. Cuadrado, V. Dikan, J. Ferrer, J. Gale, P. García-Fernández, V.M. García-Suárez, S. García, G. Huhs, S. Illera, R. Korytár, P. Koval, I. Lebedeva, L. Lin, P. López-Tarifa, S.G. Mayo, S. Mohr, P. Ordejón, A. Postnikov, Y. Pouillon, M. Pruneda, R. Robles, D. Sánchez-Portal, J.M. Soler, R. Ullah, V.W.-z. Yu, J. Junquera, J. Chem. Phys. 152 (2020) 204108.
[13] M.J. Han, T. Ozaki, J. Yu, Phys. Rev. B 73 (2006) 045110.
[14] X. Qu, P. Xu, H. Jiang, L. He, X. Ren, J. Chem. Phys. 156 (2022) 234104.
[15] D. Sánchez-Portal, E. Artacho, J.M. Soler, Solid State Commun. 95 (1995) 685.
[16] F. Bultmark, F. Cricchio, O. Grånäs, L. Nordström, Phys. Rev. B 80 (2009) 035121.
[17] J.D. Jackson, Classical Electrodynamics, John Wiley & Sons, New York, 1975.
[18] A. Messiah, Mécanique Quantique, Dunod, Paris, 1960.
[19] F.M.F. de Groot, J.C. Fuggle, B.T. Thole, G.A. Sawatzky, Phys. Rev. B 42 (1990) 5459.
[20] L. Vaugier, Electronic Structure of Correlated Materials from First Principles: Hubbard interaction and Hund's exchange, Ph. d. Thesis, École Polytechnique, 2011.
[21] B. Amadon, T. Applencourt, F. Bruneval, Phys. Rev. B 89 (2014) 125110, Phys. Rev. B 96 (2017) 199907.
[22] J.P. Perdew, K. Burke, M. Ernzerhof, Phys. Rev. Lett. 77 (1996) 3865.
[23] J.P. Perdew, A. Ruzsinszky, G.I. Csonka, O.A. Vydrov, G.E. Scuseria, L.A. Constantin, X. Zhou, K. Burke, Phys. Rev. Lett. 100 (2008) 136406.
[24] R. Cuadrado, J.I. Cerdá, J. Phys. Condens. Matter 24 (2012) 086005.
[25] R. Cuadrado, K. Liu, T.J. Klemmer, R.W. Chantrell, Appl. Phys. Lett. 108 (2016) 123102.
[26] N. Troullier, J.L. Martins, Phys. Rev. B 43 (1991) 1993.
[27] L. Kleinman, D.M. Bylander, Phys. Rev. Lett. 48 (1982) 1425.
[28] O.F. Sankey, D.J. Niklewski, Phys. Rev. B 40 (1989) 3979.
[29] E. Artacho, D. Sánchez-Portal, P. Ordejón, A. García, J.M. Soler, Phys. Status Solidi (b) 215 (1999) 809.
[30] J. Junquera, O. Paz, D. Sánchez-Portal, E. Artacho, Phys. Rev. B 64 (2001) 235111.
[31] E. Anglada, J.M. Soler, J. Junquera, E. Artacho, Phys. Rev. B 66 (2002) 205101.
[32] H.J. Monkhorst, J.D. Pack, Phys. Rev. B 13 (1976) 5188.
[33] Y. Ping, G. Galli, W.A. Goddard, J. Phys. Chem. C 119 (2015) 11570.
[34] C.L. McDaniel, S.J. Schneider, J. Res. Natl. Bur. Stand. A, Phys. Chem. 71A (1967) 119.
[35] G. Kresse, J. Furthmüller, Comput. Mater. Sci. 6 (1996) 15.
[36] G. Kresse, J. Furthmüller, Phys. Rev. B 54 (1996) 11169.
[37] P.E. Blöchl, Phys. Rev. B 50 (1994) 17953.
[38] P. Giannozzi, S. Baroni, N. Bonini, M. Calandra, R. Car, C. Cavazzoni, D. Ceresoli, G.L. Chiarotti, M. Cococcioni, I. Dabo, A.D. Corso, S. de Gironcoli, S. Fabris, G. Fratesi, R. Gebauer, U. Gerstmann, C. Gougoussis, A. Kokalj, M. Lazzeri, L. Martin-Samos, N. Marzari, F. Mauri, R. Mazzarello, S. Paolini, A. Pasquarello, L. Paulatto, C. Sbraccia, S. Scandolo, G. Sclauzero, A.P. Seitsonen, A. Smogunov, P. Umari, R.M. Wentzcovitch, J. Phys. Condens. Matter 21 (2009) 395502.
[39] P. Giannozzi, O. Andreussi, T. Brumme, O. Bunau, M.B. Nardelli, M. Calandra, R. Car, C. Cavazzoni, D. Ceresoli, M. Cococcioni, N. Colonna, I. Carnimeo, A.D. Corso, S. de Gironcoli, P. Delugas, R.A. DiStasio, A. Ferretti, A. Floris, G. Fratesi, G. Fugallo, R. Gebauer, U. Gerstmann, F. Giustino, T. Gorni, J. Jia, M. Kawamura, H.-Y. Ko, A. Kokalj, E. Küçükbenli, M. Lazzeri, M. Marsili, N. Marzari, F. Mauri, N.L. Nguyen, H.-V. Nguyen, A.O. de-la Roza, L. Paulatto, S. Poncé, D. Rocca, R. Sabatini, B. Santra, M. Schlipf, A.P. Seitsonen, A. Smogunov, I. Timrov, T. Thonhauser, P. Umari, N. Vast, X. Wu, S. Baroni, J. Phys. Condens. Matter 29 (2017) 465901.
[40] D. Vanderbilt, Phys. Rev. B 41 (1990) 7892.
[41] A. Dal Corso, Comput. Mater. Sci. 95 (2014) 337.
[42] J.M. Kahk, C.G. Poll, F.E. Oropeza, J.M. Ablett, D. Céolin, J.-P. Rueff, S. Agrestini, Y. Utsumi, K.D. Tsuei, Y.F. Liao, F. Borgatti, G. Panaccione, A. Regoutz, R.G. Egdell, B.J. Morgan, D.O. Scanlon, D.J. Payne, Phys. Rev. Lett. 112 (2014) 117601.